

Journal of
Mechanics of
Materials and Structures

**NUMERICAL MODELING OF CRACK PROPAGATION IN ROCKS
UNDER TBM DISC CUTTERS**

Mohammad Fatehi Marji, Hasan Hosseini Nasab
and Amin Hossein Morshedi

Volume 4, N^o 3

March 2009



mathematical sciences publishers

NUMERICAL MODELING OF CRACK PROPAGATION IN ROCKS UNDER TBM DISC CUTTERS

MOHAMMAD FATEHI MARJI, HASAN HOSSEINI NASAB AND AMIN HOSSEIN MORSHEDI

The mechanism of rock fragmentation underneath disc cutters is not fully understood although a number of experimental and numerical investigations have been carried out in this field. Linear elastic fracture mechanics is widely applied for the analysis of crack problems in rock mechanics. In this study, the higher order displacement discontinuity method is modified for the analysis of crack problems using the cubic variations of displacement discontinuities and three special crack tip elements. It is shown how a new formulation of the indirect boundary element method known as the displacement discontinuity method (DDM) can be used to determine the stress intensity factors of the cracks produced in rocks underneath disc cutters of tunnel boring machines (TBMs). Crack initiation angles and propagation paths in the rock can also be predicted using this numerical procedure and a mixed mode fracture criterion (for example, the maximum tensile stress criterion). In this numerical approach, three special crack tip elements are used to increase the accuracy of the displacement discontinuities near the crack tips. This method has been used to find approximately the effect of the specific disc parameters (except speed) on the thrust force, the rolling force, and the specific energy. Crack propagation in rocks under disc cutters is numerically modeled and an optimum ratio of disc spacing to penetration depth of about 10 is obtained, in good agreement with the theoretical and experimental results in the literature.

1. Introduction

Tunnel boring machines (TBMs) are usually equipped with disc cutters. The most dominant fracture process involved in cutting by TBMs is due to the subsurface crack propagation and interaction, or subsurface chipping, between adjacent cutters. The chipping process is due to forces from the multiple disc cutters mounted on the cutting head of the machines on the rock face. Several experimental, empirical, analytical and semianalytical models have been used for TBM performance prediction, such as those developed by the Earth Mechanics Institute of the Colorado School of Mines, the University of Trondheim and the Norwegian Institute of Technology, and the Department of Mining Engineering at the Technical University of Istanbul [Lislerud 1988; Nilsen and Ozdemir 1993; Rostami et al. 1994; Johanessen 1995; Bilgin et al. 2000]. Other experimental and theoretical research and work has also been reported for the investigation of the mechanism of rock fragmentation underneath the disc cutters, but its true mechanism is not fully understood yet [Roxborough and Phillips 1975; Howarth and Roxborough 1982; Snowdon et al. 1982; Tan et al. 1996].

Keywords: crack analysis, cubic elements, semi-infinite problems, displacement discontinuity method, crack tip elements, disc cutters.

Several attempts have been made to use fracture mechanics principles via boundary element methods (especially the displacement discontinuity method), for the simulation of rock fracture mechanics problems [Guo et al. 1992; Whittaker et al. 1992; Shen and Stephansson 1994; Alehossein et al. 2000; Bobet 2001]. In this study, fracture mechanics principles are implemented in the higher order (third order) displacement discontinuity method modified for crack problems. The cubic variations of displacement discontinuity and three special crack tip elements for each crack tip are used for the discretization of the boundary of the problem. The rock breakage mechanism under disc cutters of tunnel boring machines (TBMs) is modeled and studied by the proposed method. The displacement discontinuity solution based on three special crack tip elements is thoroughly explained and the required formulations are derived and given in the text.

Fundamentally, there are three mixed mode fracture criteria: the maximum tangential stress fracture criterion (or σ -criterion), the maximum strain energy release rate fracture criterion (or G -criterion), and the minimum strain energy density fracture criterion (or S -criterion) [Erdogan and Sih 1963; Ingraffea 1983; Huang and Wang 1985; Ouchterlony 1988; Broek 1989]. The recent fracture codes, such as FRACOD, which is based on the two-dimensional displacement discontinuity method, uses the modified version of Griffith's G -criterion (the F -criterion) to describe the fracture propagation processes [Shen and Stephansson 1994]. All of the mixed mode fracture criteria can be implemented in the proposed higher order displacement discontinuity method. However, the fracture propagation process predicted using the σ -criterion lies between those processes predicted using the other two classic criteria [Ingraffea 1983; Whittaker et al. 1992]: the G -criterion is more conservative and the S -criterion is less. (Note that the K_{IC} predicted by the S -criterion depends on the material parameter of the Poisson's ratio ν .)

In this paper, crack propagation analysis is accomplished by using a suitable mixed mode fracture criterion, the maximum tangential stress criterion (or σ -criterion) of [Erdogan and Sih 1963]. This simple mixed mode criterion, used by several researchers [Ingraffea 1983; Guo et al. 1992; Whittaker et al. 1992; Bobet 2001], compares the computed Mode I and Mode II stress intensity factors K_I and K_{II} with K_{IC} and K_{IIC} , Mode I and Mode II fracture toughness values under plane strain condition [Erdogan and Sih 1963; Ingraffea 1983; Huang and Wang 1985; Ouchterlony 1988; Broek 1989; Whittaker et al. 1992].

A good deal of research [Stephansson et al. 2001; Stephansson 2002; Backers et al. 2002; 2003; Rao et al. 2003; Backers 2004; Backers et al. 2004; Shen et al. 2004] has shown that the Mode II fracture toughness of rock material is usually higher than the Mode I fracture toughness, especially when the confining pressure increases. It also showed that the rocks are stronger under confining pressure, and that usually crack propagation occurs in Mode II loading under this condition [Backers 2004]. Backers et al. 2002 described a new experimental method for determination of Mode II (shear) fracture toughness of rock, K_{IIC} , and compared the outcome to results from Mode I (tensile) fracture toughness, K_{IC} , using the International Society of Rock Mechanics chevron bend test method.

Fracture toughness describes the resistance of rock to fracturing. This parameter is therefore important in estimating the failure of rock and rock structures using rock fracture mechanics principles. In this study, wedge-shaped cracks under mixed mode loading conditions are considered. These cracks are produced on a free surface of a semi-infinite rock mass by forcing the disc cutters onto the rock. As the confining pressure near the rock surface is negligible, the cracks will propagate mostly by mixed mode loading.

The displacement discontinuity solution used in the analysis presented here is of third order, which gives very accurate results of the displacement discontinuity variations along the general boundary elements with only two degrees of freedom. Because of the singularities of the displacement discontinuities at the crack tips, special crack tip elements have been proposed and used in the literature, but in most cases only one or two crack tip elements have been used. To obtain a more accurate result of the near crack tip displacement discontinuities, three or more crack tip elements can be used. This increases computation time, but not to a significant extent for modern computers. Therefore, the displacement discontinuity solution based on three general special crack tip elements is thoroughly explained and given here.

2. The cubic variation of displacement discontinuity element

A displacement discontinuity element of length $2a$ along the x -axis (Figure 1, left) is characterized by a general displacement discontinuity distribution $D(\varepsilon)$. By taking D_x and D_y components of the general displacement discontinuity $D(\varepsilon)$ to be constant in the interval $(-a, +a)$ as shown in Figure 1, right, the constant element displacement discontinuities D_x and D_y are defined as [Crouch 1976]

$$\begin{aligned} D_x &= u_x(x, 0_-) - u_x(x, 0_+), \\ D_y &= u_y(x, 0_-) - u_y(x, 0_+), \end{aligned} \tag{1}$$

where $u_x(x, 0_-)$, $u_y(x, 0_-)$, $u_x(x, 0_+)$, and $u_y(x, 0_+)$ are the x and y components of displacements in the negative side of y ($y = 0_-$) and positive side of y ($y = 0_+$), respectively.

The general displacement discontinuity method and its formulation for the constant and the higher elements (using equal subelements) are explained in the literature [Crouch 1976; Crawford and Curran 1982; Crouch and Starfield 1983; Shou and Crouch 1995; Fatehi Marji et al. 2006]. In the present paper, the general linear and cubic variations (subelements may or may not be equal) of the displacement discontinuity method are discussed, and their numerical results are compared with each other.

The linear element displacement discontinuity is based on analytical integration of linear collocation shape functions over collinear straight-line displacement discontinuity elements. Figure 2, left, shows the linear displacement discontinuity distribution, which can be written in a general form as

$$D_i(\varepsilon) = N_{1L}(\varepsilon)D_i^1 + N_{2L}(\varepsilon)D_i^2, \quad i = x, y, \tag{2}$$

where D_i^1 and D_i^2 are the linear nodal displacement discontinuities.

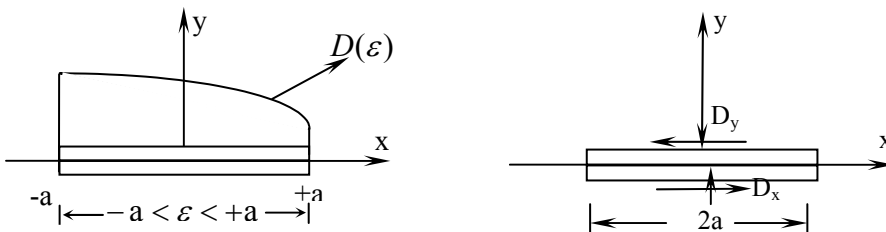


Figure 1. Left: Displacement discontinuity element and the distribution of $u(\varepsilon)$. Right: Constant element displacement discontinuity and positive sign convention.

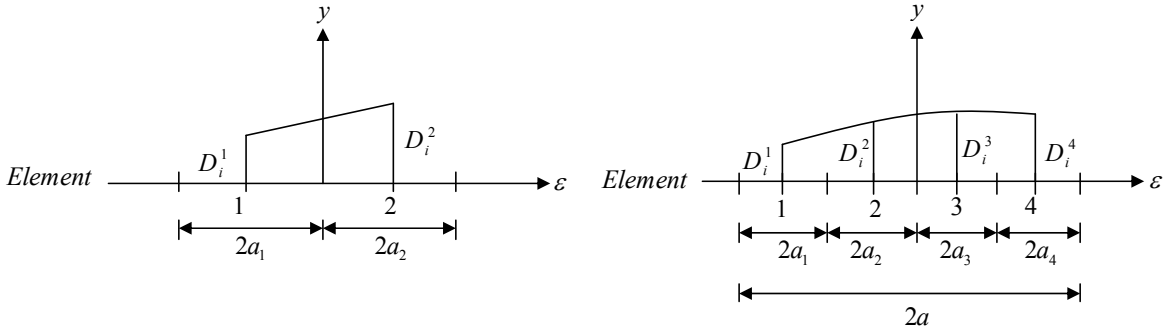


Figure 2. Linear (left) and cubic (right) collocations for the higher order displacement discontinuity variations.

The linear shape functions $N_{1L}(\varepsilon)$ and $N_{2L}(\varepsilon)$ can be defined as

$$N_{1L}(\varepsilon) = -\frac{\varepsilon - a_2}{a_1 + a_2}, \quad N_{2L}(\varepsilon) = \frac{\varepsilon + a_1}{a_1 + a_2}, \quad (3)$$

which are their linear collocation shape functions. Note that a linear element has two nodes, the centers of its two subelements.

Similarly, the cubic element displacement discontinuity is based on analytical integration of cubic collocation shape functions over collinear straight-line displacement discontinuity elements. Figure 2, right, shows the cubic displacement discontinuity distribution, which can be written as

$$D_i(\varepsilon) = \sum_{j=1}^4 N_j(\varepsilon) D_i^j, \quad i = x, y, \quad (4)$$

where D_i^1 , D_i^2 , D_i^3 , and D_i^4 are the cubic nodal displacement discontinuities, and the cubic collocation shape functions $N_j(\varepsilon)$ can be defined as

$$N_j(\varepsilon) = \sum_{j=1}^4 (A_j + B_j \varepsilon + C_j \varepsilon^2 + D_j \varepsilon^3), \quad (5)$$

where the constants A_j , B_j , C_j and D_j are successively defined by the following equalities:

$$A_1 = a_2 B_1 - a_2^2 C_1 + a_2^3 D_1, \quad A_2 = 1 + a_2 B_2 - a_2^2 C_2 + a_2^3 D_2,$$

$$A_3 = a_2 B_3 - a_2^2 C_3 + a_2^3 D_3, \quad A_4 = a_2 B_4 - a_2^2 C_4 + a_2^3 D_4,$$

$$B_1 = (a_2 - a_3) C_1 - (a_2^2 - a_2 a_3 + a_3^2) D_1, \quad B_2 = -\frac{1}{a_2 + a_3} + (a_2 - a_3) C_2 - (a_2^2 - a_2 a_3 + a_3^2) D_2,$$

$$B_3 = \frac{1}{a_2 + a_3} + (a_2 - a_3) C_3 - (a_2^2 - a_2 a_3 + a_3^2) D_3, \quad B_4 = (a_2 - a_3) C_4 - (a_2^2 - a_2 a_3 + a_3^2) D_4,$$

$$C_1 = C_{20}(1 + C_{2D} D_1), \quad C_2 = C_{20}(C_{22} + C_{2D} D_2), \quad C_3 = C_{20}(C_{31} + C_{2D} D_3), \quad C_4 = C_{2D} D_4,$$

$$D_1 = \frac{D_{1N}}{D_D}, \quad D_2 = \frac{D_{2N}}{D_D}, \quad D_3 = \frac{D_{3N}}{D_D}, \quad D_4 = \frac{D_{10}}{D_D}, \quad D_D = 1 - D_{10} D_{1C} C_{10} C_{1D},$$

$$C_{10} = \frac{1}{(2a_2 + a_1)(a_1 + a_2 + a_3) - a_2a_3}, \quad C_{11} = \frac{a_2}{a_2 + a_3}, \quad C_{12} = -\frac{2a_2 + a_1}{a_2 + a_3}, \quad C_{13} = \frac{a_1 + a_2}{a_2 + a_3},$$

$$C_{20} = \frac{1}{(2a_2 + a_1)^2 - a_2^2 - (a_1 + a_2)(a_2 - a_3)}, \quad C_{22} = -\frac{a_1 + 2a_2 + a_3}{a_2 + a_3}, \quad C_{23} = \frac{a_1 + a_2}{a_2 + a_3},$$

$$C_{1D} = -(2a_2 + a_1)((a_2^2 - a_2a_3 + a_3^2) - (2a_2 + a_1)^2),$$

$$C_{2D} = (2a_2 + a_1)^3 - a_2^3 - (a_1 + a_2)(a_2^2 - a_2a_3 + a_3^2),$$

$$D_{1N} = D_{10}(D_{11} + D_{1C}C_{10}C_{11}), \quad D_{2N} = D_{10}(D_{12} + D_{1C}C_{10}C_{12}), \quad D_{3N} = D_{10}(D_{13} + D_{1C}C_{10}C_{13}),$$

$$D_{10} = \frac{1}{(2a_3 + a_4)^3 + a_2a_3(a_2 - a_3) - (2a_3 + a_4)(a_2^2 - a_2a_3 + a_3^2)}, \quad D_{11} = -\frac{a_3}{a_2 + a_3},$$

$$D_{12} = \frac{2a_3 + a_4}{a_2 + a_3}, \quad D_{13} = -\frac{a_2 + 2a_3 + a_4}{a_2 + a_3}, \quad D_{1C} = a_2a_3 - (2a_3 + a_4)(a_2 + a_3 + a_4).$$

A cubic element has four nodes, the centers of its four subelements (Figure 2). For the special case $a_1 = a_2 = a_3 = a_4$, the general shape functions given by (5) reduce to [Fatehi Marji et al. 2007]

$$N_1(\varepsilon) = -\frac{3a_1^3 - a_1^2\varepsilon - 3a_1\varepsilon^2 + \varepsilon^3}{48a_1^3}, \quad N_2(\varepsilon) = \frac{9a_1^3 - 9a_1^2\varepsilon - a_1\varepsilon^2 + \varepsilon^3}{16a_1^3},$$

$$N_3(\varepsilon) = \frac{9a_1^3 + 9a_1^2\varepsilon - a_1\varepsilon^2 - \varepsilon^3}{16a_1^3}, \quad N_4(\varepsilon) = -\frac{3a_1^3 + a_1^2\varepsilon - 3a_1\varepsilon^2 - \varepsilon^3}{48a_1^3}. \tag{6}$$

Crouch [1976] expressed the displacements for a line crack in an infinite body along the x -axis in terms of single harmonic functions $g(x, y)$ and $f(x, y)$ as

$$u_x = 2(1 - \nu)f_{,y} - yf_{,xx} - (1 - 2\nu)g_{,x} - yg_{,xy}, \quad u_y = (1 - 2\nu)f_{,x} - yf_{,xy} + 2(1 - \nu)g_{,y} - yg_{,yy}, \tag{7}$$

while the corresponding stresses are

$$\sigma_{xx} = 2\mu(2f_{,xy} + yf_{,xyy} + g_{,yy} + yg_{,yyy}),$$

$$\sigma_{yy} = 2\mu(-yf_{,xyy} + g_{,yy} - yg_{,yyy}),$$

$$\sigma_{xy} = 2\mu(2f_{,yy} + yf_{,yyy} - yg_{,xyy}).$$
(8)

Here μ is the shear modulus, ν is Poisson’s ratio, and the subscript comma denotes partial differential with respect to the following variable(s). These potential functions for the cubic element case can be found from

$$f(x, y) = \frac{-1}{4\pi(1 - \nu)} \sum_{j=1}^4 D_x^j F_j(x, y), \quad g(x, y) = \frac{-1}{4\pi(1 - \nu)} \sum_{j=1}^4 D_y^j F_j(x, y), \tag{9}$$

where

$$F_j(x, y) = \int_{-a}^a N_j(\varepsilon) \ln \sqrt{(x - \varepsilon)^2 + y^2} d\varepsilon. \quad j = 1, 2, 3, 4, \tag{10}$$

Using the coefficients in (6), one can write the F_j in terms of the integrals

$$I_k(x, y) = \int_{-a}^a \varepsilon^k \ln \sqrt{(x - \varepsilon)^2 + y^2} d\varepsilon, \quad (11)$$

whose explicit expressions are, in terms of the auxiliary quantities $\theta_1 = \arctan \frac{y}{x-a}$, $\theta_2 = \arctan \frac{y}{x+a}$, $r_1 = \sqrt{(x-a)^2 + y^2}$, and $r_2 = \sqrt{(x+a)^2 + y^2}$, given by

$$I_0(x, y) = y(\theta_1 - \theta_2) - x \ln \frac{r_1}{r_2} + a \ln(r_1 r_2) - 2a, \quad (12a)$$

$$I_1(x, y) = xy(\theta_1 - \theta_2) + \frac{y^2 - x^2 + a^2}{2} \ln \frac{r_1}{r_2} - ax, \quad (12b)$$

$$I_2(x, y) = \frac{y}{3}(3x^2 - y^2)(\theta_1 - \theta_2) + \frac{3xy^2 - x^3}{3} \ln \frac{r_1}{r_2} + \frac{a^3}{3} \ln(r_1 r_2) - \frac{6ax^2 - 6ay^3 + 2a^3}{9}, \quad (12c)$$

$$I_3(x, y) = -xy(x^2 - y^2)(\theta_1 - \theta_2) + \frac{3x^4 - 6x^2y^2 + 8a^2x^2 + a^4 - y^4}{4} \ln \frac{r_1}{r_2} - 2ax(x^2 + a^2) \ln(r_1 r_2) + \frac{9ax^3 - 18axy^2 + 7a^3x}{6}. \quad (12d)$$

As discussed, the boundary and crack of any specified problem are discretized by N elemental finite line segments. Let D_s^j and D_n^j be the shear and normal components of the nodal displacement discontinuities given in (4) for each boundary element.

The corresponding nodal stresses are

$$\begin{bmatrix} \sigma_s^i \\ \sigma_n^i \end{bmatrix} = \begin{bmatrix} A_{ss}^{ij} & A_{sn}^{ij} \\ A_{ns}^{ij} & A_{nn}^{ij} \end{bmatrix} \begin{bmatrix} D_s^j \\ D_n^j \end{bmatrix}, \quad (13)$$

where σ_n^i and σ_s^i are the normal and stress components at the i -th node, and the matrix entries (A_{ss}^{ij} , etc.) are the influence coefficients obtained by using (8)–(12). Similarly, the displacements are

$$\begin{bmatrix} u_s^i \\ u_n^i \end{bmatrix} = \begin{bmatrix} B_{ss}^{ij} & B_{sn}^{ij} \\ B_{ns}^{ij} & B_{nn}^{ij} \end{bmatrix} \begin{bmatrix} D_s^j \\ D_n^j \end{bmatrix}, \quad (14)$$

where u_n^i and u_s^i are the normal and shear displacement component, at the i -th node, and the matrix entries (B_{ss}^{ij} , etc.) are the influence coefficients obtained by using (7) and (9)–(12). By using the specified values of the stresses or displacements to the boundaries and crack of the problem, it is possible to find the required displacement discontinuities D_s^j and D_n^j at each elemental node.

3. Computation of mixed mode stress intensity factors

Consider a body of arbitrary shape with a crack subjected to mixed mode loading (that is, tensile and shear loadings). The displacements and stresses near the crack tip of a crack of arbitrary size (in a body of arbitrary shape) subjected to arbitrary tensile and shear loading are given in [Irwin 1957]. The

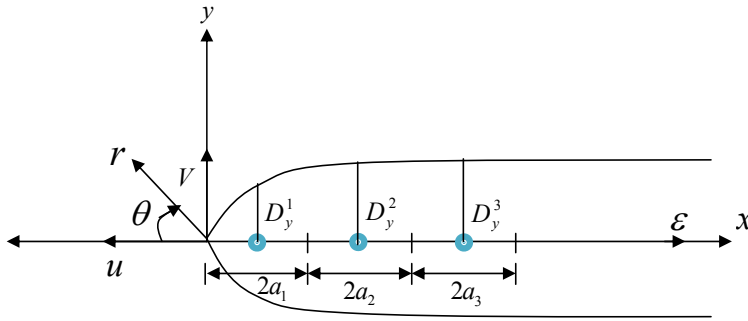


Figure 3. Special three-element crack tip for boundary collocation technique.

displacements are

$$\begin{aligned}
 u_x &= \frac{K_I}{4G} \sqrt{\frac{r}{2\pi}} \left[(2\kappa - 1) \cos \frac{\theta}{2} - \cos \frac{3\theta}{2} \right] + \frac{K_{II}}{4G} \sqrt{\frac{r}{2\pi}} \left[(2\kappa + 3) \sin \frac{\theta}{2} + \sin \frac{3\theta}{2} \right], \\
 u_y &= \frac{K_I}{4G} \sqrt{\frac{r}{2\pi}} \left[(2\kappa - 1) \sin \frac{\theta}{2} - \sin \frac{3\theta}{2} \right] - \frac{K_{II}}{4G} \sqrt{\frac{r}{2\pi}} \left[(2\kappa - 3) \cos \frac{\theta}{2} + \cos \frac{3\theta}{2} \right],
 \end{aligned} \tag{15a}$$

and the stresses are

$$\begin{aligned}
 \sigma_x &= \frac{K_I}{\sqrt{2\pi r}} \cos \frac{\theta}{2} \left[1 - \sin \frac{\theta}{2} \sin \frac{3\theta}{2} \right] - \frac{K_{II}}{\sqrt{2\pi r}} \sin \frac{\theta}{2} \left[2 + \cos \frac{\theta}{2} \cos \frac{3\theta}{2} \right] + \dots, \\
 \sigma_y &= \frac{K_I}{\sqrt{2\pi r}} \cos \frac{\theta}{2} \left[1 + \sin \frac{\theta}{2} \sin \frac{3\theta}{2} \right] + \frac{K_{II}}{\sqrt{2\pi r}} \sin \frac{\theta}{2} \cos \frac{\theta}{2} \cos \frac{3\theta}{2} + \dots, \\
 \sigma_{xy} &= \frac{K_I}{\sqrt{2\pi r}} \sin \frac{\theta}{2} \cos \frac{\theta}{2} \cos \frac{3\theta}{2} + \frac{K_{II}}{\sqrt{2\pi r}} \cos \frac{\theta}{2} \left[1 - \sin \frac{\theta}{2} \sin \frac{3\theta}{2} \right] + \dots,
 \end{aligned} \tag{15b}$$

where $\kappa = (3 - 4\nu)$ for plane strain and $\kappa = (3 - \nu)/(1 + \nu)$ for plane stress, K_I and K_{II} are the Mode I and Mode II stress intensity factors, and r and θ are polar coordinates defined as in [Figure 3](#).

The displacement discontinuity method allows crack surfaces to be discretized and computes the normal displacement discontinuity (crack opening displacement) and the shear displacement discontinuity (crack sliding displacement) directly as part of the solution for each element. Based on LEFM (linear elastic fracture mechanics) theory, the Mode I and Mode II stress intensity factors K_I and K_{II} can be written from [\(1\)](#) and [\(15a\)](#) in terms of the normal and shear displacement discontinuities as

$$K_I = \frac{\mu}{4(1 - \nu)} \sqrt{\frac{2\pi}{a}} D_y(a), \quad K_{II} = \frac{\mu}{4(1 - \nu)} \sqrt{\frac{2\pi}{a}} D_x(a). \tag{16}$$

In previous work, usually one or two special crack tip elements have been used [[Shou and Crouch 1995](#); [Fatehi Marji et al. 2006](#)]. In the present paper, three special crack tip elements are used, to achieve better accuracy for the displacement discontinuities near the crack ends, and in particular to model the $1/\sqrt{r}$ behavior of [\(15b\)](#), characteristic of the stress field in the near field region of the crack tip.

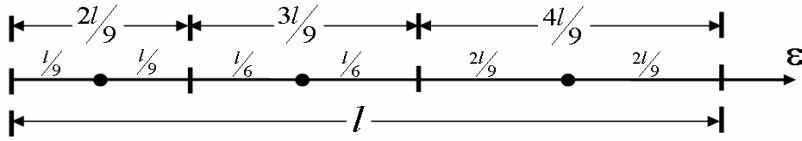


Figure 4. The three special crack tip element lengths $l_1 = 2a_1 = \frac{2}{9}l$, $l_2 = 2a_2 = \frac{3}{9}l$, and $l_3 = 2a_3 = \frac{4}{9}l$.

Consider a crack tip of length $l = 2a = 2(a_1 + a_2 + a_3)$ in an infinite isotropic elastic body, as shown in [Figure 3](#). Omitting details, which can be found in [\[Fatehi Marji et al. 2006\]](#), the variation of displacement discontinuities along this crack tip element can be written as

$$D_i(\varepsilon) = N_{C1}(\varepsilon)D_i^1(a) + N_{C2}(\varepsilon)D_i^2(a) + N_{C3}(\varepsilon)D_i^3(a), \quad (17)$$

where the functions N_{Cj} are given below.

We first consider the subelement lengths $l_1 = 2a_1 = \frac{2}{9}l$, $l_2 = 2a_2 = \frac{3}{9}l$, and $l_3 = 2a_3 = \frac{4}{9}l$, as shown in [Figure 4](#). The general shape functions $N_{C1}(\varepsilon)$, $N_{C2}(\varepsilon)$, and $N_{C3}(\varepsilon)$ of (17) in this case are

$$N_{C1}(\varepsilon) = \frac{(a_{22} - a_{33})(a_{22}a_{33}\varepsilon^{1/2} - (a_{22} + a_{33})\varepsilon^{3/2} + \varepsilon^{5/2})}{a_{11}^{1/2}(a_{11} - a_{22})(a_{11}a_{22} - a_{11}a_{33} - a_{22}a_{33} + a_{33}^2)}, \quad (18a)$$

$$N_{C2}(\varepsilon) = \frac{(a_{33} - a_{11})(a_{11}a_{33}\varepsilon^{1/2} - (a_{11} + a_{33})\varepsilon^{3/2} + \varepsilon^{5/2})}{a_{22}^{1/2}(a_{11} - a_{22})(a_{11}a_{22} - a_{11}a_{33} - a_{22}a_{33} + a_{33}^2)}, \quad (18b)$$

$$N_{C3}(\varepsilon) = \frac{a_{11}a_{33}\varepsilon^{1/2} - (a_{11} + a_{33})\varepsilon^{3/2} + \varepsilon^{5/2}}{a_{33}^{1/2}(a_{11}a_{22} - a_{11}a_{33} - a_{22}a_{33} + a_{33}^2)}, \quad (18c)$$

where $a_{11} = a_1 = \frac{1}{9}l$, $a_{22} = 2a_1 + a_2 = \frac{7}{18}l$, and $a_{33} = 2(a_1 + a_2) + a_3 = \frac{7}{9}l$.

If instead we take $a_1 = a_2 = a_3$, the shape functions $N_{C1}(\varepsilon)$, $N_{C2}(\varepsilon)$, and $N_{C3}(\varepsilon)$ become (see [\[Fatehi Marji et al. 2007\]](#))

$$N_{C1}(\varepsilon) = \sqrt{\frac{\varepsilon}{a_1}} \left(\frac{15}{8} - \frac{\varepsilon}{a_1} + \frac{\varepsilon^2}{8a_1^2} \right), \quad (19a)$$

$$N_{C2}(\varepsilon) = -\sqrt{\frac{\varepsilon}{3a_1}} \left(\frac{5}{4} - \frac{3\varepsilon}{2a_1} + \frac{\varepsilon^2}{4a_1^2} \right), \quad (19b)$$

$$N_{C3}(\varepsilon) = \sqrt{\frac{\varepsilon}{5a_1}} \left(\frac{3}{8} - \frac{\varepsilon}{2a_1} + \frac{\varepsilon^2}{8a_1^2} \right). \quad (19c)$$

Substituting (18) or (19) into (17), and then substituting these equations into (7) and (8), and working as in the derivation of the general potential functions F_j in (10), we can obtain the general potential function $f_C(x, y)$ for the crack tip element as

$$f_C(x, y) = \frac{-1}{4\pi(1-\nu)} \sum_{j=1}^3 D_i^j \int_{-a}^a N_j(\varepsilon) \ln \sqrt{(x-\varepsilon)^2 + y^2} d\varepsilon, \quad (20)$$

which can conveniently be written in terms of the integrals

$$I_{Ck}(x, y) = \int_{-a}^a \varepsilon^{k-\frac{1}{2}} \ln \sqrt{(x-\varepsilon)^2 + y^2} d\varepsilon, \quad k = 1, 2, 3 \quad (21)$$

using the coefficients of powers of ε given in (18) or (19).

Two degrees of freedom are used for each node at the center of each subelement, as explained in [Shou and Crouch 1995].

4. Crack initiation and propagation

Based on LEFM principles, a crack will start propagation in the direction of the crack initiation angle $\theta = \theta_0$ [Ingraffea 1983]. (See Figure 3 for notation.) Several mixed mode fracture criteria have been proposed for the estimation of this angle [Ingraffea 1983; Broek 1989; Whittaker et al. 1992], the main three being the maximum tangential stress criterion or σ -criterion, the maximum strain energy release rate criterion or G -criterion, and the minimum strain energy density criterion or S -criterion. Modified forms of these criteria (for example, the F -criterion, which derives from the G -criterion) have also been used in the fracture mechanics literature [Ingraffea 1983; Broek 1989; Whittaker et al. 1992; Stephansson 2002].

All these criteria have demonstrated that a crack in a plate under a general in-plane load does not initiate and propagate in its original plane, that is, $\theta_0 \neq 0$. In brittle substances (like most rocks), although fracture of Mode II plays an important role under certain loading conditions and Mode I fracture toughness (K_{IC}) is less than that of Mode II (K_{IIC}), due to weakness (low strength) under tension the rock breaks due to tensile stress. In most such cases, the influence of K_{IC} prevails over that of K_{IIC} under pure tensile, pure shear, tension-shear, and compression-shear loading conditions [Rao et al. 2003].

To predict the crack initiation angle θ_0 and the path of crack propagation, the maximum tangential stress criterion or σ -criterion, is used here. This is one of the classical mixed mode fracture criteria which are widely used by several researchers [Ingraffea 1983; Guo et al. 1992]. Based on this criterion, the crack will start its propagation when the critical maximum tangential tensile stress σ_{θ_0} (in the direction of the crack propagation angle θ_0) satisfies the following condition [Ingraffea 1983; Guo et al. 1992; Whittaker et al. 1992]:

$$\sigma_{\theta_0} = \frac{1}{\sqrt{2\pi r}} \cos \frac{\theta_0}{2} \left[K_I \sin \frac{\theta_0}{2} \cos \frac{\theta_0}{2} + K_{II} \left(1 - 3 \sin^2 \frac{\theta_0}{2} \right) \right] = 0. \quad (22)$$

From this equation, the crack propagation angle θ_0 can be estimated as

$$\theta_0 = 2 \tan^{-1} \left(\frac{K_I}{4K_{II}} \pm \frac{1}{4} \sqrt{\frac{K_I^2}{K_{II}^2} + 8} \right) \text{ for } K_{II} \neq 0 \quad \text{and} \quad \theta_0 = 0 \text{ for } K_{II} = 0. \quad (23)$$

Finally, the general form of the σ -criterion in term of the Mode I fracture toughness of the material, (K_{IC}), and the crack propagation angle θ_0 can be expressed as

$$\cos \frac{\theta_0}{2} \left[K_I \cos^2 \frac{\theta_0}{2} - \frac{3}{2} K_{II} \sin \frac{\theta_0}{2} \right] = K_{IC} \text{ (or } 0.866K_{II}). \quad (24)$$

In the present paper, Equations (22), (23), and (24) are used for a given crack length b (or a central crack length $2b$). To predict the crack propagation path, the original crack of length b is extended by

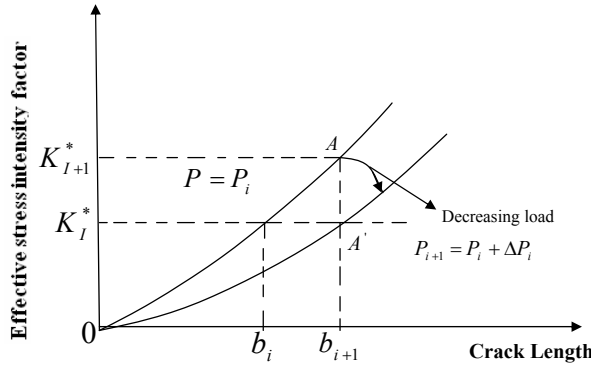


Figure 5. Variation of effective stress intensity with crack length [Ingraffea 1983].

an amount Δb so that a new crack length $b + \Delta b$ is obtained, and again (22), (23), and (24) are used to predict the new conditions of crack propagation for this new crack. This procedure is repeated until the crack stops its propagation or the material breaks away. This procedure can give a propagation path for a given crack under a certain loading condition. Considering the effective (or normalized) stress intensity factor $K_{IC}^* = K_I/K_{IC}$, Figure 5 shows the stress intensity variation with crack length for any in-plane crack problem. The load level $P_{i+1} = (K_{IC}/K_{I+1})P_i$ can be computed for each crack increment length, Δb [Ingraffea 1983]. Therefore, a new algorithm is added to the main displacement discontinuity program to evaluate the effective stress intensity factor $K_{IC}^* = K_I/K_{IC}$ and a new crack propagation angle θ_0 in each iteration.

5. A pressurized center crack in an infinite plane

As an example, the pressurized crack problem shown in Figure 6 is solved numerically by the proposed method. The numerical results are compared with those results obtained analytically by [Sneddon 1951]. As shown in Figure 6, a center crack of length $2b$ in an infinite plane is subjected to a uniform pressure p . The analytical solution for the normal displacement discontinuity D_y along the crack boundary and the normal stress σ_y near the crack tip ($|x| > b$) can be written as

$$D_y = -\frac{2(1-\nu)P}{\mu} \sqrt{b^2 - x^2} \text{ if } |x| > b \quad \text{and} \quad \sigma_y = \frac{Px}{\sqrt{x^2 - b^2}} - P \text{ if } |x| < b. \quad (25)$$

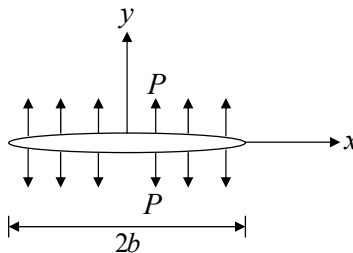


Figure 6. A pressurized crack in an infinite plane.

Number of elements	Distance from crack tip	$D_y(a)/b \times 10^3$			
		Analytical solution	Ordinary elements	One special crack tip element	Three special crack tip elements
4	0.25	-1.1906	-1.5463	-1.3275	-1.2092
10	0.1	-0.7846	-0.9964	-0.8569	-0.8168
20	0.05	-0.5621	-0.7089	-0.6104	-0.5874
40	0.025	-0.4000	-0.5029	-0.4332	-0.4183

Table 1. Displacement discontinuity $D_y(a)/b \times 10^3$ at the center $x = a$ of an element at the crack tip using ordinary elements, one special crack tip element and three special crack tip elements.

In the following analysis, a pressurized crack problem with half crack length $b = 1$ m, normal pressure $P = -10$ MPa, modulus of elasticity $E = 2.2$ GPa, and Poisson’s ratio $\nu = 0.1$ is considered.

Table 1 compares the different values of the normalized displacement discontinuity distribution D_y/b along the surface of the pressurized crack using the constant (ordinary) displacement discontinuity program TWODD with three crack tip elements [Crouch and Starfield 1983]. As shown in this table, by using only one special crack tip element, the percent error of displacement discontinuity D_y at a distance $x = 0.05b$ from the crack tip is reduced from 26.12% to 8.59%, and by using three special crack tip elements it is reduced to 4.5%.

If the same problem is solved using 15 cubic elements (60 nodes) with the proposed method, the percentage error of displacement discontinuity D_y at a distance $x = 0.05b$ from the crack tip will be 5.23% (without the special crack tip elements), and the results obtained by using the constant element displacement discontinuity method (the TWODD program) with the same number of nodes (60 constant elements) gives an error of 24.17% [Crouch and Starfield 1983]. Table 2 compares the variation of the normalized displacement discontinuity D_y/b along the surfaces of a pressurized crack using ordinary (constant element) and higher order (cubic element) displacement discontinuity methods. The results given in Tables 1 and 2 demonstrate that although all displacement discontinuity results are very close to their corresponding analytical values, those using three special crack tip elements are somewhat superior.

6. Edge cracks in a half plane

Edge crack problems in a half plane can also be solved using the cubic element formulation, but a proper mixed-mode fracture criterion such as that one explained in Section 3 should be implemented in the program to investigate the crack propagation direction and its propagation path. Figure 7 shows the oblique edge cracks with different inclination angles β on a traction-free half plane. For the problem shown in Figure 7, the inclination angle is $\beta = 45^\circ$, the crack length is $b = 1$ m, and the ratio of the crack tip element length, l , to crack length, b , is 0.1 (that is, $l/b = 0.1$). The normalized stress intensity factors $K_I/(\sigma\sqrt{\pi b})$ and $K_{II}/(\sigma\sqrt{\pi b})$ for this particular problem can be estimated from the results given by [Bowie 1973] as 0.729 and 0.371, respectively.

x/b	$D_y/b \times 10^3$				
Distance from the crack tip	Analytical Results	Constant Elements (TWODD)	Error (%)	Cubic Elements	Error (%)
0.000	3.980	4.046	1.66	3.985	0.13
0.086	3.946	4.032	2.18	3.957	0.28
0.171	3.901	3.989	2.26	3.914	0.33
0.257	3.827	3.916	2.33	3.839	0.31
0.343	3.720	3.812	2.47	3.736	0.43
0.429	3.578	3.673	2.66	3.589	0.31
0.514	3.396	3.497	2.97	3.407	0.32
0.600	3.168	3.276	3.41	3.182	0.44
0.686	2.882	3.000	4.09	2.897	0.52
0.771	2.520	2.654	5.33	2.536	0.62
0.857	2.040	2.203	7.99	2.073	1.60
0.950	1.237	1.536	24.17	1.289	4.20

Table 2. Comparison of displacement discontinuity $D_y/b \times 10^3$ along the surface of a pressurized crack using ordinary (constant) elements and higher order elements for displacement discontinuity methods without using a special crack tip element.

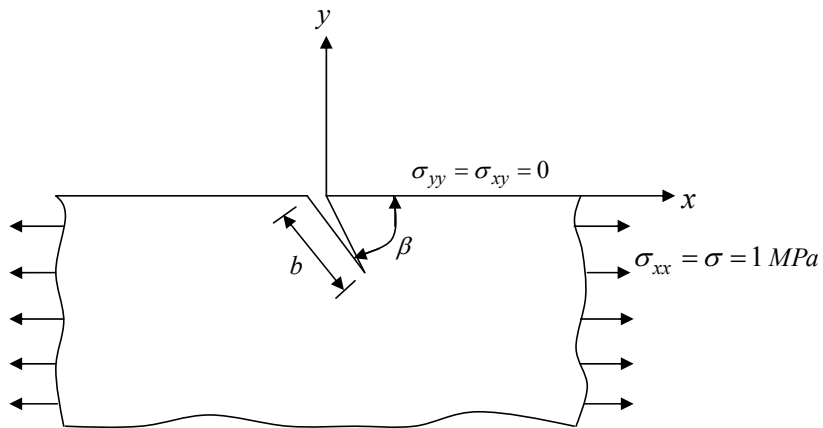


Figure 7. Oblique edge cracks in a semi-infinite plane.

The numerical results for the same problem are obtained by using the displacement discontinuity method for a traction-free half plane with different kind of elements, that is, ordinary elements (constant elements), quadratic elements, and the new cubic elements presented in this study. Table 3 shows the effect of the number of elements along the cracks using a constant $l/b = 0.1$, and taking sufficient elements (48 nodes) along the boundary of the problem (it should be noted that three special crack tip elements are used for obtaining these results).

Number of nodes	$K_I/(\sigma\sqrt{\pi b})$				$K_{II}/(\sigma\sqrt{\pi b})$			
	Constant elements	Error (%)	Cubic elements	Error (%)	Constant elements	Error (%)	Cubic elements	Error (%)
12	0.775	6.310	0.742	1.783	0.398	7.278	0.379	2.156
24	0.768	5.350	0.736	0.960	0.390	5.121	0.376	1.348
36	0.763	4.664	0.735	0.547	0.388	4.582	0.375	1.078
48	0.760	4.252	0.734	0.410	0.387	4.312	0.374	0.809
60	0.759	4.115	0.734	0.410	0.386	4.043	0.373	0.539

Table 3. Analytical and numerical values of the Mode I and Mode II stress intensity factors $K_I/(\sigma\sqrt{\pi b})$ and $K_{II}/(\sigma\sqrt{\pi b})$ for the 45° oblique edge crack using different number of elements along the crack ($l/b = 0.1$).

l/b	$K_I/(\sigma\sqrt{\pi b})$				$K_{II}/(\sigma\sqrt{\pi b})$			
	Constant elements	Error (%)	Cubic elements	Error (%)	Constant elements	Error (%)	Cubic elements	Error (%)
0.05	0.764	4.801	0.732	0.137	0.390	5.121	0.370	-0.270
0.10	0.760	4.252	0.734	0.410	0.388	4.582	0.373	0.540
0.15	0.758	3.978	0.735	0.547	0.386	4.043	0.372	0.270
0.20	0.759	4.115	0.729	-0.274	0.387	4.312	0.374	0.809
0.25	0.760	4.252	0.727	-0.547	0.388	4.582	0.375	1.078

Table 4. Analytical and numerical values of the Mode I and Mode II stress intensity factors $K_I/(\sigma\sqrt{\pi b})$ and $K_{II}/(\sigma\sqrt{\pi b})$ for the 45° oblique edge crack using different l/b ratios.

Table 4 shows the effect of the crack tip element length, l , on the normalized stress intensity factors $K_I/(\sigma\sqrt{\pi b})$ and $K_{II}/(\sigma\sqrt{\pi b})$. The results given in this table are obtained using a constant number of nodes (48, 12 cubic elements) along the crack. The results presented in Tables 3 and 4 demonstrate the accuracy and effectiveness of the proposed method.

7. Crack propagation mechanisms due to disc cutters in a semi-infinite rock mass

Disc cutters over the surface of a continuous rock mass are shown schematically in Figures 10 and 11. It is assumed that the disc cutters have diameter D , disc edge angle φ , penetration depth P_d , and spacing S . The thrust force F_t is required to maintain the disc at the desired depth of penetration, and the rolling force F_r is also necessary to keep the disc rolling at this penetration depth. Specific energy E_S (in MJ/m³ in three dimensions or in MPa/m² in two dimensions) is a measure of the amount of energy that is required for breaking the rock under the disc cutter. Penetration depth P_d , disc edge angle φ , disc diameter D , spacing S , and speed are the primary variables related to disc cutters. Roxborough and Phillips [1975] showed that the specific energy E_S and rolling force F_r are nearly independent of the disc diameter, but the thrust force F_t increases with an increase of disc diameter.

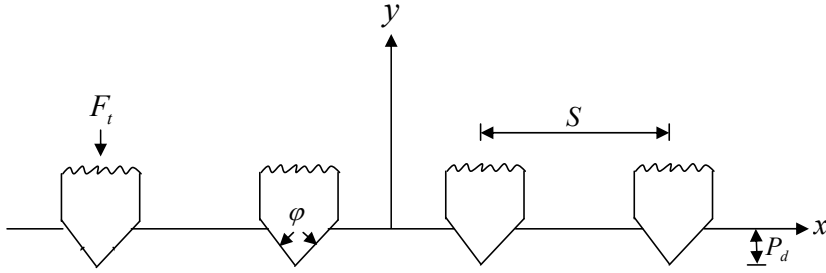


Figure 8. Side view of four equally spaced rows of disc cutters over the surface of a continuous rock mass.

In this section we use the semi-infinite displacement discontinuity method for crack analysis using cubic elements (SDDMCAC), with three special crack tip elements at each crack end, to find the approximate effects of the thrust force F_t , the rolling force F_r , and the specific energy E_S , for a constant disc diameter D (for example, $D = 432$ mm) on the penetration depth P_d and the disc spacing S . We consider a typical TBM with a thrust of 250 kN per cutter, with disc cutters of 15 mm width and 432 mm diameter [Roxborough and Phillips 1975]. The typical rock is Aspo diorite, with $K_{IC} = 3.83$ MPa m^{1/2} and $K_{IIC} = 5.09$ MPa m^{1/2} [Backers 2004]. The other parameters of this rock, as reported in the same source, are $\sigma_t = 15$ MPa, $\sigma_C = 220$ MPa, $E = 68$ GPa, and $\nu = 0.24$.

The symmetric problem of four rows of disc cutters is shown in Figure 8. Taking into account the symmetry of each wedge about a vertical plane, simple trigonometry shows that the normal and shear forces along each side of the groove equal, respectively, $(F_t/2) \cos(\phi/2)$ and $(F_t/2) \sin(\phi/2)$, while the length b of the side of the cut is $b = P_d / \cos(\phi/2)$. Assuming strain conditions, we therefore obtain for the normal and shear components of stresses along the crack length b

$$\sigma_n = F_t \frac{\cos(\phi/2)}{2bl}, \quad \sigma_s = F_t \frac{\sin(\phi/2)}{2bl}. \quad (26)$$

The values of the normal and shear stresses along these cracks are determined by fixing the normal stress at an assumed value and calculating the shear stress from the geometry of the wedge. By changing the value of normal stress and its corresponding shear stress and checking whether the crack starts its propagation or not, it is possible to predict the minimum value of the normal and shear stresses at which the crack propagation begins. Then, the minimum values of the thrust force F_t can be evaluated from (26) for different disc edge angles ϕ .

The rolling force F_r can be estimated from the thrust force F_t through the formula

$$F_r = \frac{F_t}{\sqrt{(D - P_d)/P_d}}, \quad (27)$$

(see [Roxborough and Phillips 1975]), where D is the diameter of the disc cutter, taken here as 432 mm.

The primary crack propagation due to disc cutters, used here to investigate the effect of adjacent disc cutters on the penetration of cracks and the formation of major chips can be modeled as in Figure 9 [Guo et al. 1992; Whittaker et al. 1992]. The effect of the penetration depth P_d on the minimum value of the

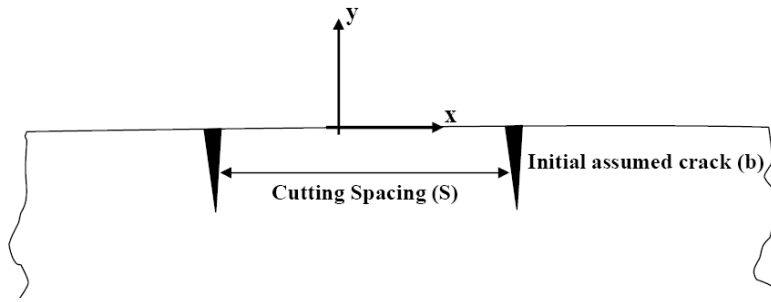


Figure 9. Geometry of adjacent disc cutters showing the cutting spacing S and initial assumed crack length b on a semi-infinite rock mass [Whittaker et al. 1992].

thrust force F_t and the corresponding rolling force F_r (which are needed to start the propagation of the crack) are obtained numerically for $\varphi = 80, 90,$ and 100° , and disc spacing $S = 30$ mm.

The numerical results for thrust force F_t and rolling force F_r , for different penetration depths P_d , and for three different disc edge angles, $\varphi = 80, 90,$ and 100° are given in Table 5. The numerical results obtained here are normalized and verified by those given experimentally in [Bilgin et al. 2000] for $\varphi = 90^\circ$ in Figure 10, which shows good agreement between numerical and experimental values.

The specific energy E_s for each disc cutter can be estimated numerically from the formula [Howarth and Roxborough 1982]

$$E_s = F_r / Q, \tag{28}$$

where Q is the extracted volume (area in two dimensions) of the rock measured in m^3 . In all of the analysis here, a constant disc edge angle $\varphi = 90^\circ$ and penetration depth $P_d = 6$ mm are considered to estimate the value of the extracted area Q which is theoretically very difficult to evaluate. The geometry of the problem considered here is shown in Figure 11, in which each side of the cut (wedge) is considered to be a separate crack. The four cracks CR_1 – CR_4 , from left to right in this figure, are solved numerically and the crack propagation angle θ_0 for each crack has been calculated in five different steps. In each step the crack length in the direction of θ_0 is extended between 1 mm and 4 mm (depending on the S/P_d ratio).

	$\varphi = 80^\circ$		$\varphi = 90^\circ$		$\varphi = 100^\circ$	
P_d (mm)	F_t (kN)	F_r (kN)	F_t (kN)	F_r (kN)	F_t (kN)	F_r (kN)
2	74.045	5.005	79.804	6.412	82.540	5.589
4	112.406	10.911	117.123	11.489	130.173	12.853
6	142.878	17.623	152.453	18.231	172.172	20.873
8	171.916	24.025	183.230	25.785	197.281	29.569
10	193.114	30.436	207.987	31.897	224.549	34.754
12	213.986	35.719	231.012	39.125	245.167	41.895

Table 5. The minimum thrust force F_t and rolling force F_r corresponding to different penetration depths P_d for disc spacing $S = 30$ mm and different disc edge angles φ .

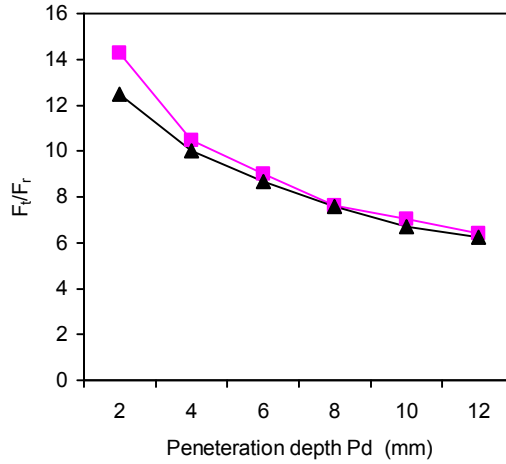


Figure 10. Comparison of the relation between F_t/F_r and P_d for a disc edge angle of 90° : pink squares, results from Table 5; black triangles, results from [Bilgin et al. 2000].

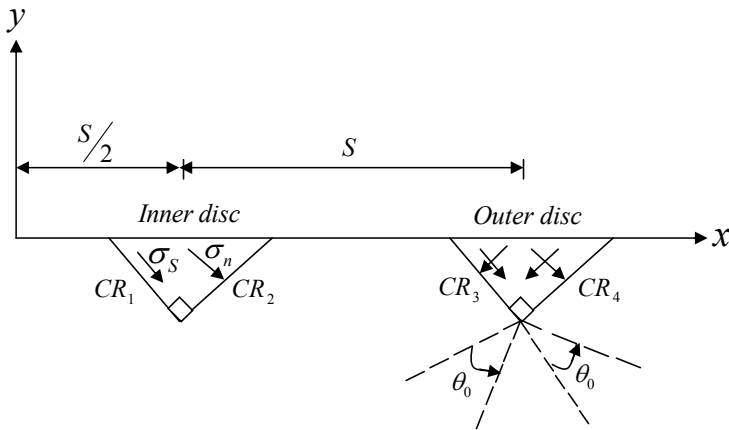


Figure 11. Symmetrical 90° disc cutters. Four cracks CR_1 – CR_4 are shown from left to right.

Step	CR_1	CR_2	CR_3	CR_4
0	-68.95	51.18	-69.14	51.27
1	-27.89	8.51	-33.37	7.87
2	-23.85	10.13	-9.36	15.17
3	12.48	33.63	-2.15	18.14
4	-18.26	17.65	-8.98	11.79
5	-4.44	22.99	-8.65	13.42

Table 6. Numerical values of crack propagation angle θ_0 (in degrees) for $S/P_d = 15$ for a 90° disc cutter. $P_d = 6$ mm and crack increment $\Delta b = 4$ mm (5 increments).

A ratio of crack tip element length l to crack length b , that is, $l/b = 0.1$, is used for the analysis of these cracks. We have taken 10 cubic elements along each original crack length and 2 cubic elements along each crack increment, and a crack tip element (with three subelements or three special crack tip elements) is added to the last crack increment. As the S/P_d ratio is one of the most important parameters in studying the mechanism of rock breaking due to disc cutters, different values of this parameter are considered here. As an example, the results obtained for $S/P_d = 15$ showing the crack propagation angle θ_0 are given in Table 6. Approximate values of the extracted area Q are obtained by finding the area restricted by the crack propagation path. The numerical values of the extracted area Q (mm^2) are estimated from the area under the crack propagation paths, for example, from those shown in Figures 12 and 13. The cracks labeled CR_1 and CR_2 are related to the inner disc, which represent its breaking

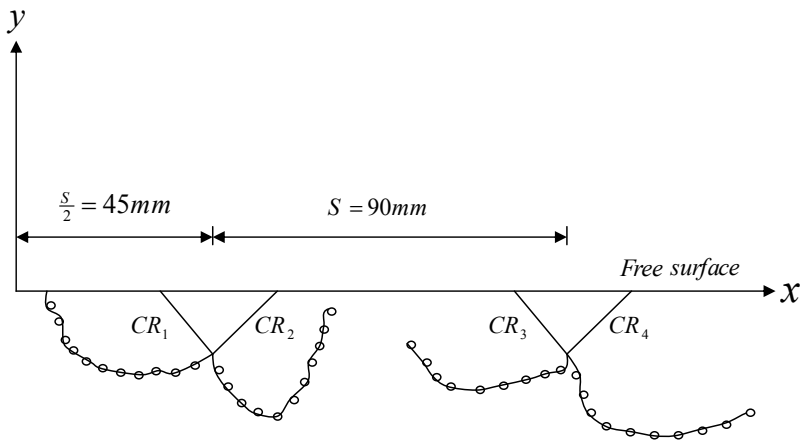


Figure 12. The crack propagation path for $S/P_d = 15$, for a 90° disc cutter, $P_d = 6$ mm, and crack increment $\Delta b = 4$ mm.

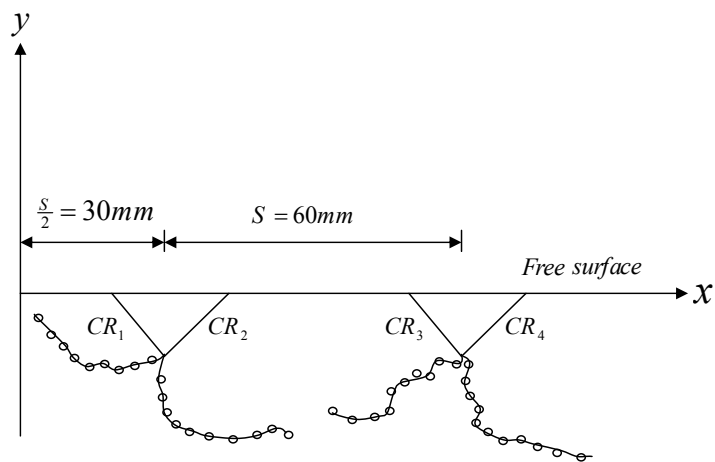


Figure 13. The crack propagation path for $S/P_d = 10$, for a 90° disc cutter, $P_d = 6$ mm, and crack increment $\Delta b = 4$ mm.

S/P_d	σ_n (MPa)	F_t (kN)	F_r (kN)	Q (mm ²)	E_s (MJ/m ³)
3.33	-56	1344	159.53	176	906.42
5.00	-51	1224	145.29	352	412.76
6.67	-44	1056	125.35	451	277.94
8.33	-35	840	99.71	676	147.50
10.00	-39	936	111.10	903	123.03
11.67	-40	960	113.95	802	142.08
13.33	-41	984	116.80	751	155.53
15.00	-43	1032	122.49	676	181.20

Table 7. Estimated values of thrust force F_t , rolling force F_r , extracted area Q , and specific energy E_s for $\Delta b = 1, 2$ and 4 mm, for different S/P_d ratios.

action. Here only the inner disc force and the area associated with this disc are used in estimating the final extracted area (Figure 14). Assuming a unit thickness for the rock, the specific energy E_s can be evaluated for different values of the ratio S/P_d (Figure 15).

In this analysis, the crack length b is increased incrementally by an amount Δb , and, correspondingly, the normal stress σ_n and shear stress σ_s are also increased to provide the sufficient energy for the crack to propagate in the direction of θ_0 . As a result of increasing the stresses at the crack boundaries, the crack starts its propagation, then a new crack length increment with 2 cubic elements and 3 crack tip elements is added in the propagation direction θ_0 , and the procedure is repeated for each crack increment Δb . Some estimated values for the forces F_t and F_r in kN, extracted area Q in mm², and specific energy E_s in MJ/m³ are tabulated in Tables 5 and 6 and also illustrated in Figures 14 and 15.

Table 7 shows that the thrust force is high for small disc spacing, and after reaching a minimum value it again increases to a larger value for very large disc spacing. Previous experimental work showed a steadily increasing thrust force with S/P_d ratio [Roxborough and Phillips 1975]. However, the model presented here is based on the propagation of existing cracks. These cracks require higher forces to propagate for smaller disc spacing due to the confinement effect of the adjacent cutters. As a result, higher forces are required to propagate the cracks for smaller disc spacings.

Figure 14, left, shows that the the thrust force F_t (kN) decreases as the S/P_d reaches about 10, but after this value it increases slowly. Figure 14, right, illustrates that the maximum extracted area that can be achieved occurs at $S/P_d = 10$. As shown in Figure 15, left, the optimum S/P_d ratio is between 8 and 15, which is in good agreement with the experimental results reported in [Roxborough and Phillips 1975; Howarth and Roxborough 1982].

Figure 15, right, illustrates the effect of the angle φ on the specific energy E_s . These results show that E_s increases with the increase in the angle φ (especially for the disc edge angles above 90°).

8. Discussion

The tunnel boring machine (TBM) is a full-face excavator which cuts rock by means of disc cutters mounted on a circular revolving cutting head. The TBM breaks rock with disc cutters mounted on its rotating cutter-head in such a pattern that they roll against the rock of the tunnel face in a series of

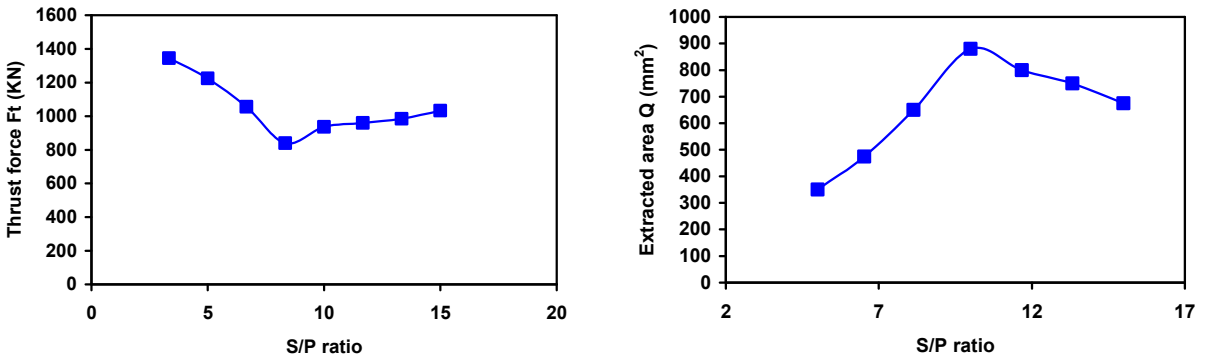


Figure 14. Estimated values of the thrust force F_t (left) and extracted area Q (right) for different S/P_d ratios.

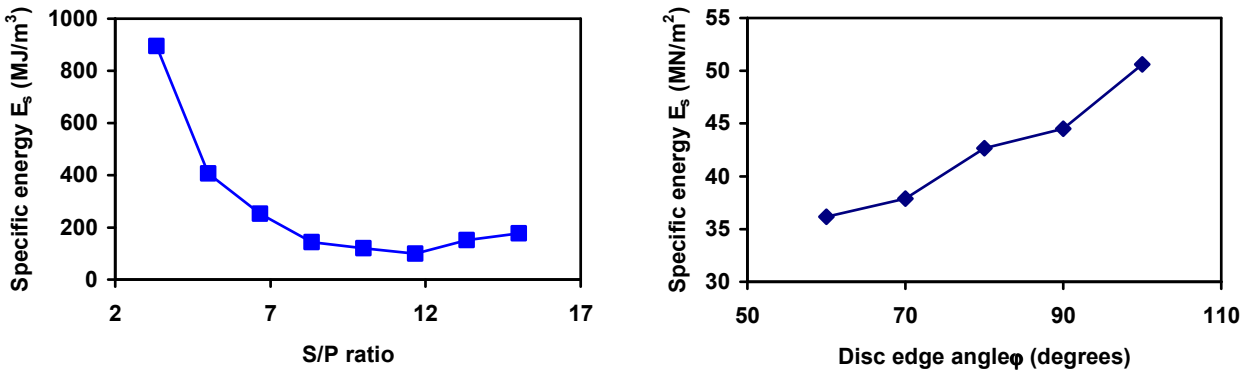


Figure 15. Specific energy E_s as a function of S/P_d at a constant F_r (left), and as a function of the disc edge angle ϕ (right).

concentric circular grooves. The cutting force is produced by powerful hydraulic thrust rams. Each disc cutter is free to rotate within its mounting manifold. To maintain contact with the rock and to maintain the optimum spacing between cutting grooves, the machine is held stable by a combination of its great mass and by hydraulic jacks acting against the side of the tunnel.

It should be noted that there is no single universally accepted theory for the formation of rock chips by indenter tools. Most of the researches believe that the main cause of rock breakage is the propagation of tensile fractures, but the mechanism by which these fractures are first initiated is somewhat uncertain. Actually, rock breakage takes place because a tensile fracture is initiated and propagated. This fracture is induced as a result of combined loading (or mixed loadings), including the tensile extension of preexisting flaws along the fracture plane and tensile stresses induced by the crushed zone beneath the wedge. Hood and Roxborough [1992] describes a model for disc cutters developed by Lindqvist and Ranman [1980] which assumes that most of the force is directed normally into the rock, similar to the action of a flat-bottomed punch. Induced tensile stresses generate cracks that run nearly parallel to the rock surface, and if the spacing between the cutters is sufficiently small, tensile cracks propagating from each groove will join up to form a rock chip.

In the analysis proposed here, to simulate the cutting mechanism of the TBM disc cutters, each cutting groove is chosen as a single original crack and two successive grooves with varying spacing are simulated. The grooves are assumed to be vertical, although inclined grooves can also be easily modeled. In the displacement discontinuity method, each side of the crack can be discretized separately, and one of the crack surfaces can be considered as a fictitious boundary (this is one of the main advantages of the indirect boundary element methods). The higher order displacement discontinuity used here considers a cubic variation of the displacement discontinuities along each element on the boundary of the problem and also along the crack boundaries (except the crack tips) which results in very accurate general displacement discontinuities. The higher order crack tip elements are also used here to obtain more accurate results of the mixed mode stress intensity factors near the crack ends, where crack propagation begins. Although rock breakage theory predicts that tensile fractures are first initiated and then propagated, fractures are induced as a result of combined loading, where the action of the shear loading should also be taken into account.

If one only considers the tensile fracture and first mode of loading, propagated cracks may not theoretically meet each other or the rock surfaces, a prediction which deviates from experimental results and the reality of cheap formation processes. Therefore, in the analysis given in this study, one of the well-known mixed mode fracture criteria (the σ -criterion) has been used. All three fundamental mixed mode I-II fracture criteria can be used for the analysis. The σ -criterion is used based on the fracture toughness envelopes given by Whittaker et al. [1992], as shown schematically in Figure 16.

Here, the problem of a crack propagation mechanism under disc cutters is modeled in such a manner that the various effective parameters such as the thrust force, S/P_d ratio, the specific energy, etc. for various cases can be obtained. The numerical results are compared with those cited in the literature, and some good results are gained. For example, the results given in Table 6 show that the thrust force is high for small disc spacing, and after reaching minimum value, it again increases to a larger value for very large disc spacing. However, the model presented here is based on the propagation of existing cracks. These cracks require higher forces to propagate for smaller spacing due to the confinement effect of the adjacent cutters. As a result, for smaller disc spacing, higher forces are required to propagate the cracks. We see from Figure 14 that the thrust force F_t (kN) decreases as S/P_d approaches 10, but subsequently increases slowly.

Figure 14, right, indicates that the maximum achievable extracted area occurs at $S/P_d = 10$. As shown in Figure 15, left, the optimum S/P_d ratio ranges from 8 to 15. Figure 15, right, illustrates the effect of the angle φ on specific energy E_s . These results show that E_s increases with an increase in the angle φ (especially for the disc edge angles above 90°).

9. Conclusion

In this work, crack propagation mechanisms under disc cutters are numerically modeled and studied using the higher order displacement discontinuity method. To increase the accuracy of displacement discontinuities near crack tips, three special crack tip elements are used for the treatment of each crack end. The maximum tangential stress fracture criterion is employed to investigate the crack propagation and its direction under disc cutters, and some of the computed results are compared with previously reported experimental results. This comparison shows that in most of the cases, the numerical results

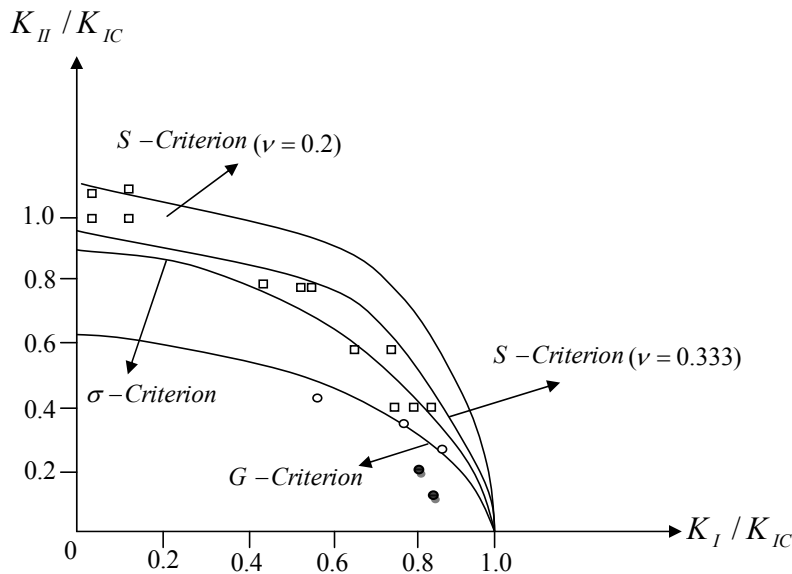


Figure 16. Fracture toughness envelopes based on various mixed mode fracture criteria [Whittaker et al. 1992]. Plotted experimental points taken [Ingraffea 1983] (open squares; Westerly granite), [Huang and Wang 1985] (black circles), and [Sun 1990] (open circles).

are in good agreement with their corresponding experimental values. As a result, for small disc spacing ($S/P_d < 6$), higher forces (more energy) are required to propagate cracks for inner discs, and for large disc spacing ($S/P_d > 15$), the specific energy E_s increases slowly because the extracted area Q tends to be constant as the spacing is increased. However, the optimum S/P_d ratio is between 8 and 15, as was expected from comparison to experimental results [Roxborough and Phillips 1975; Howarth and Roxborough 1982; Lislrud 1988; Nilsen and Ozdemir 1993; Rostami et al. 1994; Johanessen 1995; Bilgin et al. 2000]. It is also concluded that as the disc edge angle ϕ increases, the specific energy E_s increases.

References

- [Alehossein et al. 2000] H. Alehossein, E. Detournay, and H. Huang, "An analytical model for the indentation of rocks by blunt tools", *Rock Mech. Rock Eng.* **33**:4 (2000), 267–284.
- [Backers 2004] T. Backers, *Fracture toughness determination and micromechanics of rock under mode I and mode II loading*, Ph.D. Thesis, university of Potsdam, Potsdam, DE, 2004, Available at <http://opus.kobv.de/ubp/volltexte/2005/229/>.
- [Backers et al. 2002] T. Backers, O. Stephansson, and E. Rybacki, "Rock fracture toughness testing in mode II punch-through shear test", *Int. J. Rock Mech. Min.* **39**:6 (2002), 755–769.
- [Backers et al. 2003] T. Backers, N. Fardin, G. Dresen, and O. Stephansson, "Effect of loading rate on mode I fracture toughness, roughness and micromechanics of sandstone", *Int. J. Rock Mech. Min.* **40**:3 (2003), 425–433.
- [Backers et al. 2004] T. Backers, G. Dresen, E. Rybacki, and O. Stephansson, "New data on mode II fracture toughness of rock from the punch-through shear test", *Int. J. Rock Mech. Min.* **41**:3 (2004), 351–352. SINOROCK2004 Paper 1A 01.

- [Bilgin et al. 2000] N. Bilgin, C. Balcı, O. Acaroğlu, H. Tunçdemir, and c. Eskikaya, “Development of rapid excavation technologies for the Turkish mining and tunnelling industries”, NATO TU Excavation project report, Istanbul Technical University, Faculty of Mines, Mining Engineering Department, 2000. pp. 172.
- [Bobet 2001] A. Bobet, “A hybridized displacement discontinuity method for mixed mode I-II-III loading”, *Int. J. Rock Mech. Min.* **38**:8 (2001), 1121–1134.
- [Bowie 1973] O. L. Bowie, “Solutions of plane crack problems by mapping techniques”, in *Methods of analysis and solutions of crack problems. Recent developments in fracture mechanics. Theory and methods of solving crack problems*, edited by G. C. Sih, Mechanics of fracture **1**, Noordhoff International, Leyden, 1973.
- [Broek 1989] D. Broek, *The practical use of fracture mechanics*, 4th ed., Kluwer, Dordrecht, 1989.
- [Crawford and Curran 1982] A. M. Crawford and J. H. Curran, “Higher-order functional variation displacement discontinuity elements”, *Int. J. Rock Mech. Min.* **19**:3 (1982), 143–148.
- [Crouch 1976] S. L. Crouch, “Solution of plane elasticity problems by the displacement discontinuity method, I: infinite body solution”, *Int. J. Numer. Methods Eng.* **10**:2 (1976), 301–343.
- [Crouch and Starfield 1983] S. L. Crouch and A. M. Starfield, *Boundary element methods in solid mechanics: with applications in rock mechanics and geological engineering*, Allen and Unwin, London, 1983.
- [Erdogan and Sih 1963] F. Erdogan and G. C. Sih, “On the crack extension in plates under plane loading and transverse shear”, *J. Basic Eng. (ASME)* **85** (1963), 519–527.
- [Fatehi Marji et al. 2006] M. Fatehi Marji, H. Hosseini-Nasab, and A. H. Kohsary, “On the uses of special crack tip elements in numerical rock fracture mechanics”, *Int. J. Solids Struct.* **43**:6 (2006), 1669–1692.
- [Fatehi Marji et al. 2007] M. Fatehi Marji, H. Hosseini-Nasab, and A. H. Kohsary, “A new cubic element formulation of the displacement discontinuity method using three special crack tip elements for crack analysis”, *JP J. Solids Struct.* **1**:1 (2007), 61–91.
- [Guo et al. 1992] H. Guo, N. I. Aziz, and L. C. Schmidt, “Rock cutting study using linear elastic fracture mechanics”, *Eng. Fract. Mech.* **41**:5 (1992), 771–778.
- [Hood and Roxborough 1992] M. C. Hood and F. F. Roxborough, “Rock breakage: mechanical”, Chapter Chapt 9.1, pp. 680–721 in *SME mining engineering handbook*, vol. 1, edited by H. L. Hartman, Society for Mining, Metallurgy and Exploration, Littleton, CO, 1992.
- [Howarth and Roxborough 1982] D. F. Howarth and F. F. Roxborough, “Some fundamental aspects of the use of disc cutters in hard-rock excavation”, *J. South Afric. Inst. Min. Metall.* (1982), 309–315.
- [Huang and Wang 1985] J. Huang and S. Wang, “An experimental investigation concerning the comprehensive fracture toughness of some brittle rocks”, *Int. J. Rock Mech. Min.* **22**:2 (1985), 99–104.
- [Ingraffea 1983] A. R. Ingraffea, “Numerical modeling of fracture propagation”, pp. 151–208 in *Rock fracture mechanics*, edited by H. P. Rossmanith, Springer-Verlag, Wien, New York, 1983.
- [Irwin 1957] G. R. Irwin, “Analysis of stresses and strains near the end of a crack traversing a plate”, *J. Appl. Mech. (ASME)* **24**:3 (1957), 361–364.
- [Johanessen 1995] O. Johanessen, “Hard rock tunnel boring”, University of Trondheim, the Norwegian Institute of Technology, 1995. p.165.
- [Lindqvist and Ranman 1980] P. E. Lindqvist and K. E. Ranman, “Mechanical rock fragmentation: chipping under a disc cutter”, Technical report 59T, University of Lulea, Lulea, Sweden, 1980.
- [Lislerud 1988] A. Lislerud, “Hard rock tunnel boring: prognosis and costs”, *Tunn. Undergr. Space Technol.* **3**:1 (1988), 9–17.
- [Nilsen and Ozdemir 1993] B. Nilsen and L. Ozdemir, “Hard rock tunnel boring prediction and field performance”, in *Rapid excavation and tunneling conference (RETC) proceedings*, edited by L. D. Bowerman and J. E. Monsees, Boston, 1993. Chapter 52.
- [Ouchterlony 1988] F. Ouchterlony (coordinator), “Suggested methods for determining the fracture toughness of rock”, *Int. J. Rock Mech. Min.* **25**:2 (1988), 71–96.
- [Rao et al. 2003] Q. Rao, Z. Sun, O. Stephansson, C. Li, and B. Stillborg, “Shear fracture (mode II) of brittle rock”, *Int. J. Rock Mech. Min.* **40**:3 (2003), 355–375.

- [Rostami et al. 1994] J. Rostami, L. Ozdemir, and M. D. Neil, “Performance prediction: a key issue in mechanical hard rock mining”, *Min. Eng.* **11** (1994), 1263–1267.
- [Roxborough and Phillips 1975] F. F. Roxborough and H. R. Phillips, “Rock excavation by disc cutter”, *Int. J. Rock Mech. Min.* **12**:12 (1975), 361–366.
- [Shen and Stephansson 1994] B. Shen and O. Stephansson, “Modification of the G -criterion for crack propagation subjected to compression”, *Eng. Fract. Mech.* **47**:2 (1994), 177–189.
- [Shen et al. 2004] B. Shen, O. Stephansson, M. Rinne, H.-S. Lee, L. Jing, and K. Roshoff, “A fracture propagation code and its applications to nuclear waste disposal”, *Int. J. Rock Mech. Min.* **41**:3 (2004), 448–449. SINOROCK2004 Paper 2B 02.
- [Shou and Crouch 1995] K. J. Shou and S. L. Crouch, “A higher order displacement discontinuity method for analysis of crack problems”, *Int. J. Rock Mech. Min.* **32**:1 (1995), 49–55.
- [Sneddon 1951] I. N. Sneddon, *Fourier transforms*, McGraw-Hill, New York, 1951.
- [Snowdon et al. 1982] R. A. Snowdon, M. D. Ryley, and J. Temporal, “A study of disc cutting in selected british rocks”, *Int. J. Rock Mech. Min.* **19**:3 (1982), 107–121.
- [Stephansson 2002] O. Stephansson, “Recent rock fracture mechanics developments”, pp. 675–698 in 1st *Iranian Rock Mechanics Conference* (Tehran, 2002), 2002.
- [Stephansson et al. 2001] O. Stephansson, T. Backers, G. Dresen, and E. Rybacki, “Shear fracture mechanics of rocks and a new testing method for K_{IIC} ”, pp. 163–168 in *Rock mechanics: a challenge for society: proceedings of the ISRM regional symposium, EUROCK 2001* (Espoo, Finland, 2001), edited by P. Sarkka and P. Eloranta, 2001.
- [Sun 1990] G. X. Sun, *Application of fracture mechanics to mine design*, Ph.D. thesis, Department of Mining Engineering, University of Nottingham, 1990.
- [Tan et al. 1996] X. C. Tan, S. Q. Kou, and P. A. Lindqvist, “Simulation of rock fragmentation by indenters using DDM and fracture mechanics”, in *Rock mechanics: tools and techniques: proceedings of the 2nd North American Rock Mechanics Symposium, NARMS'96, a regional conference of ISRM* (Montreal, 1996), edited by M. Aubertin et al., A. A. Balkema, Rotterdam, 1996.
- [Whittaker et al. 1992] B. N. Whittaker, R. N. Singh, and G. Sun, *Rock fracture mechanics: principles, design and applications*, Elsevier, Amsterdam, 1992.

Received 31 Dec 2008. Revised 11 Mar 2009. Accepted 11 Mar 2009.

MOHAMMAD FATEHI MARJI: mfatehi@yazduni.ac.ir

Department of Mining Engineering, Yazd University, Safaiyeh, Yazd 89195741, Iran,

HASAN HOSSEINI NASAB: hhn@yazduni.ac.ir

Department of Industrial Engineering, Yazd University, Safaiyeh, Yazd 89195741, Iran,

AMIN HOSSEIN MORSHEDI: morshedy82@gmail.com

Department of Mining and Petroleum Engineering, Tehran University, Tehran, Iran